Journal of *Marine Science and Engineering*

MDPI

Article

A Nonlinear Backstepping Controller Design for High-Precision Tracking Applications with Input-Delay Gimbal Systems

Hwan-Cheol Park [1], Soumayya Chakir [2], Young-Bok Kim [3,*] and Thinh Huynh [3,*]

[1] Ship Training and Operations Center, Pukyong National University, Busan 48513, Korea; phc6028@gmail.com
[2] Department of Mechanical System Engineering, Pukyong National University, Busan 48513, Korea; soumayya.chakir@gmail.com
[3] Department of Smart Robot Convergence and Application Engineering, Pukyong National University, Busan 48513, Korea
* Correspondence: kpjiwoo@pknu.ac.kr (Y.-B.K.); huynhthinh@hcmute.edu.vn (T.H.); Tel.: +82-51-629-6197 (Y.-B.K.)

Abstract: This paper proposes a novel nonlinear control approach for a two-axis gimbal to achieve accurate real-time tracking performance in maritime surveillance applications. For this objective, the control system must overcome system complexities and limitations, including nonlinear dynamics, coupled Euler angle-based measurements, and delay time constraints. The nonlinear backstepping controller was designed, taking into consideration the nonlinearities and system couplings to preserve the system stability. Then, an extra backstep was incorporated to minimize the control errors due to the delay time. The proposed control scheme enhances the tracking performances and expands the system's bandwidth, which is validated in the simulations and experimental studies in comparison with a super-twisting sliding mode controller introduced in a previous study.

Keywords: backstepping control; Euler angles; gimbal system; input-delay system; super-twisting sliding mode

Citation: Park, H.-C.; Chakir, S.; Kim, Y.-B.; Huynh, T. A Nonlinear Backstepping Controller Design for High-Precision Tracking Applications with Input-Delay Gimbal Systems. *J. Mar. Sci. Eng.* **2021**, *9*, 530. https://doi.org/10.3390/jmse9050530

Academic Editor: Nikolaos I. Xiros

Received: 3 April 2021
Accepted: 13 May 2021
Published: 14 May 2021

1. Introduction

Gimbaled mechanisms are widely used in practical applications where the line-of-sight (LOS) of an optical sensor needs to be stabilized and steered to track a moving target. Carried on mobile vehicles, these mechanisms are electromechanical structures consisting of two or more independent channels. Each of these channels orientates about an axis different from the others. The optical sensors, such as vision and thermal cameras, radars, and laser sensors, are usually mounted on the inner channel of the gimbal. However, in some configurations, the sensors are fixed to the vehicle carrying the gimbal where mirrors or other optical elements are mounted. Moreover, a gyro or a set of gyros is used to measure rotational motions in the inertial space and feedbacks the data to the control systems. Requirements for these systems vary depending on applications. On one hand, in applications such as mapping, security, communications, and handheld cameras, the control problems mainly focus on attenuating unmeasured disturbances affecting the optical sensors. On the other hand, in target tracking, surveillance, missile guidance, gun-turret control, and astronomical telescopes applications, the sensor is required to track the target precisely in real time. The complexity of the system dynamics, unpredicted target direction, and disturbances make these tasks challenging even though control problems of gimbal systems have been studied for decades. In 2018, a special issue of IEEE Control Systems Magazine was dedicated to inertially stabilized platforms and presented several articles overviewing many aspects of this topic [1,2].

The gimbal itself is a simple structure, but its dynamics are complex with nonlinear factors, couplings, and disturbances. Mathematical models of the system have been derived

from many studies to point out these problems. In [1], the kinematics of a multi-axis gimbal was devised in terms of the trigonometric functions of the platform and rotations of the gimbal channels. Analyzing these equations highlights the kinematics coupling and unwanted effects on the LOS motion. Meanwhile, the representation of the simplest one-axis gimbal dynamics was introduced in [2], and the dynamics of the two-axis one had been derived in several studies [3]. Recent studies, such as [4–8], analyzed in detail the system models with complex nonlinearities induced by cross-couplings, parameter uncertainties, and external disturbances. Thus, there is a need to design an effective control system so that robust stability and superior performance are achieved.

In order to attain these objectives, numerous control approaches were suggested. Classical control strategies of a gimbal system proposed two control loops: an inner rate or stabilization loop inside an outer tracking loop. The inner loop compensates for disturbances, and the tracking loop ensures that the sensor LOS remains pointing towards the target [2]. Additionally, in [3], two control methods have been deployed: direct stabilization using feedback signals from the LOS orientation and indirect stabilization based on the base motion. However, modern control techniques allow the design of a single controller that can both track the target and suppress disturbances. The popular schemes used to control gimbal mechanisms are the sliding mode control (SMC), robust control, and active disturbance rejection control, thanks to their robustness and effectiveness when facing disturbances. For instance, an integral sliding mode controller combined with an observer, namely a reduced-order cascade extended state observer [6] and a disturbance/uncertainty estimator [9] were suggested. A terminal SMC and a high-order sliding mode observer were designed in [5] to overcome the cross-coupling and external disturbances that influence the system. Moreover, a backstepping sliding mode controller with an adaptive neural networks approach was designed in [7], and a super-twisting sliding mode controller (STSMC) was introduced in [10]. On the other hand, robust control theory was applied in [8,11] and several other studies. Especially, the study in [8] introduced a new robust double active control scheme for a two-axis gimbal system, where an inner active compensator was combined with a feedback controller designed based on H_∞ framework. This configuration was introduced so that the system was able to suppress both external disturbances and mutual interferences. However, the design process of most of these controllers neglected the nonlinear characteristics of the system. Instead, they were treated as unknown disturbances and estimated by an observer.

Furthermore, practical gimbal systems and their components cannot operate ideally, which can significantly affect the performance of the control systems. Actuator saturation, gyro output parameterization, and communication network may be listed among practical factors contributing to performance deterioration. However, very few studies considered them while designing the controllers. For example, the study in [7] dealt with a gimbal system with saturated actuators that degraded the system performance. Thus, the authors applied an auxiliary function to define the effect of saturation and obtained a suitable SMC law. However, the framework of this function was not thoroughly explained. Additionally, the authors in [10] considered quaternion feedback from the gyro sensor in designing a super-twisting controller for a three degrees-of-freedom (DoF) inertial stabilization platform. Generally, gyro-type sensors provide several ways to represent the 3D orientation of an object in space, namely Euler angles, quaternions, axis angles, and rotation matrices. These concepts are different from the concept of angular position, angular velocity, and angular acceleration that are usually used in motion equations. That is the feedback values from the gyros are not the ones expected by the system model.

Besides the abovementioned factors, the time delay is receiving lots of attention thanks to the increasing use of networked control systems and closed-loop actuators. In these systems, a simple controller is integrated with an actuator, and they form a servo-system that works as a node in the network. In master and slave network configurations, the main controller works as the master, while sensors and actuators are slaves. Data, including sensor feedback and control signal data, are transmitted via a shared network or wireless

connections. The study of Baillieul and Antsaklis [12] reviewed the problems of control and communication in networked real-time systems. Communication time, which introduced the delay time to the system inputs and outputs, was listed as a challenge that reduces the system performances. An overview article from Richard [13] recalled the characteristics of delay systems and summarized available approaches for their control. In this article, it was stated that the delay systems, both state or input delay, retard or neutral system, usually had bad reputations of system stability and performance. However, while most of the developed techniques have been proved to be effective for state delay systems, controlling input delay systems is more complex and difficult to deal with.

Several approaches have been suggested for input delay systems, namely predictor-like control, robust control, and sliding mode control. A classical hypothesis in the modeling of physical processes is to assume that the future behavior of the deterministic system can be summed up in its present state only. The idea of the predictor control is to establish an expression of the delay-free controller by predicting values of the state and the output ahead of time. The prediction can be achieved by either a state predictor technique, reduction transformation [14], Smith predictor technique [15], or inverse backstepping transformation [16–18]. They have been claimed to be able to achieve a globally asymptotic stability even with time-varying delays; however, the system should be simple and linear. A combination of backstepping and adaptive techniques (in [19–21]) was introduced for input-delay systems represented in a strict-feedback form with uncertainties to achieve—in the best cases—semi-uniform ultimate boundedness of systems. In addition, by taking advantage of modern hardware, more complex control techniques can be implemented with delay systems, such as aperiodic sampling [22] and model predictive controller [23]. Otherwise, by treating the difference between the current and delayed control signals as input disturbance, the control objective becomes the attenuation of the matching disturbances, which the SMC and robust control schemes are well known to be able to deal with. In [13], several research studies using these two methods have been listed, and most of the time, even matching additive disturbance cannot be completely rejected. This implies the ultimate boundedness instead of the asymptotic convergence. For example, the study in [8] used the same kind of actuators and communication network, and neither the proposed robust double active controller nor the integral sliding mode was able to effectively reject the influences of the time delay in the system. In [24], the sliding mode algorithm was used to design an observer that estimates the matching disturbances, then reconstructs the states and delays for a system with input delay. However, it is worth noting that any estimation from an observer is always lagging behind the true values for some time. Along with the available delay time in the input channel and the limitations of the system bandwidth, a combination of a controller and an observer may lead to deterioration of the system performance and the system stability. Thus, the abovementioned approaches in [4–11], where the common control technique is a combination of the main controller and an observer, might not be suitable for input-delay systems.

Therefore, a novel nonlinear controller for a two-axis gimbal system is designed in this paper to cope with the system complexities and constraints, namely nonlinear dynamic characteristics, gyros feedback parameterization, and system delays. Designed based on the backstepping technique and Lyapunov stability theory, the proposed control scheme preserves the system stability, and accurate real-time tracking performances were achieved. The design procedure of the proposed controller is presented in detail. Simulation and experimental studies were conducted to evaluate the proposed control strategy. Comparison studies were conducted between the proposed control system and an STSMC. Accordingly, the contributions of this paper are listed as follows:

- A mathematical representation of the two-axis gimbal system is derived, taking into consideration the Euler angle feedbacks and the input delay time.
- A novel nonlinear backstepping controller is introduced for the two-axis gimbal systems to overcome the abovementioned difficulties.

- Simulation and experimental results validate the effectiveness of the proposed controller.

The remainder of this paper is organized into five sections. The system mathematical model is described in Section 2. Section 3 presents the design process of the controller and stability analysis. Simulation and experimental studies are conducted in Section 4, where the frequency and time responses of the controlled system are analyzed. Finally, conclusions are drawn in Section 5.

2. System Modeling

2.1. Kinematics and Dynamics

The gimbal system considered in this paper consists of an outer channel actuating the pan motion and an inner channel operating the tilt motion. The payload, a set of cameras, is attached to the inner channel and its motion is measured by a gyros-type sensor. The sensor feedbacks consist of orientations expressed in Euler angle parameterizations and inertial angular rates. This assembly is used in marine surveillance applications, where the camera's LOS needs to be stabilized and steered to accurately track a predefined target in real time. Subsequently, it is necessary to derive the mathematical model of the system, where the outputs are given in Euler angles, and the states include Euler angles, angular rates, and angular accelerations. The configuration of a vessel-mounted gimbal system is illustrated in Figure 1, and the coordinate systems are as follows:

- OXYZ: earth fixed reference frame;
- $OX_bY_bZ_b$: platform fixed frame;
- $OX_pY_pZ_p$: pan motion channel fixed frame;
- $OX_tY_tZ_t$: tilt motion channel fixed frame.

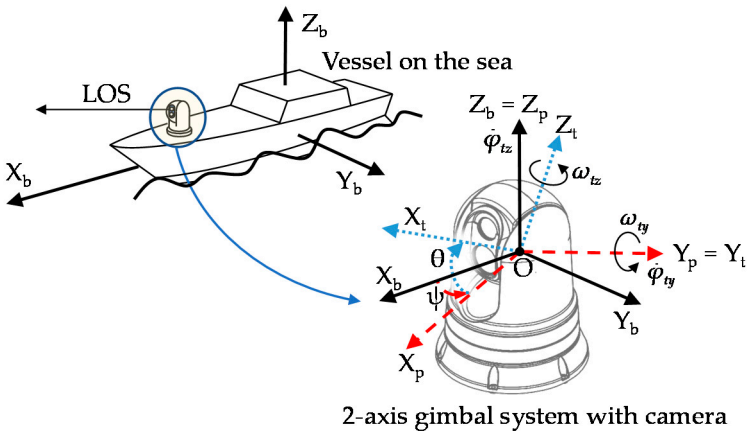

Figure 1. Schematic of a 2-axis gimbal system mounted on a vessel.

All of the coordinates are carried into coincidence at the rotational center of the tilt channel of the gimbal.

Then, the kinematics of the system are given as:

$$\begin{bmatrix} \omega_{tx} \\ \omega_{ty} \\ \omega_{tz} \end{bmatrix} = \begin{bmatrix} C\theta\left(\omega_{bx}C\psi + \omega_{by}S\psi\right) - S\theta(\omega_{bz} + \omega_{\psi}) \\ -\omega_{bx}S\psi + \omega_{by}C\psi + \omega_{\theta} \\ S\theta\left(\omega_{bx}C\psi + \omega_{by}S\psi\right) + C\theta(\omega_{bz} + \omega_{\psi}) \end{bmatrix} \tag{1}$$

where $\boldsymbol{\omega}_t = \begin{bmatrix} \omega_{tx} & \omega_{ty} & \omega_{tz} \end{bmatrix}^T$ and $\boldsymbol{\omega}_b = \begin{bmatrix} \omega_{bx} & \omega_{by} & \omega_{bz} \end{bmatrix}^T$ are the angular rate vectors of the tilt channel and those of the platform, respectively. S and C denote the sine and cosine functions. ψ is the relative motion between the outer gimbal and the platform along the Z_b-axis of the platform, θ is the relative motion between the inner and the outer gimbal along the Y_p-axis of the outer channel, while ω_{ψ} and ω_{θ} are their respective rates.

Let the orientations of the inner channel be described by three Euler angles, namely pan, tilt, and roll, in the following order:

- Rotation of φ_{tz} about the Z_t-axis of the inner channel fixed frame, followed by a
- Rotation of φ_{ty} about the Y_t-axis of the moving frame, followed by a
- Rotation of φ_{tx} about the X_t-axis of the moving frame.

By taking the angular rate of each Euler angle about the final coordinate system, the relationship between the angular rates of the tilt channel and the rates of change in the Euler angles is obtained as follows:

$$\begin{bmatrix} \dot{\varphi}_{tx} \\ \dot{\varphi}_{ty} \\ \dot{\varphi}_{tz} \end{bmatrix} = \begin{bmatrix} 1 & S\varphi_{tx}\tan\varphi_{ty} & C\varphi_{tx}\tan\varphi_{ty} \\ 0 & C\varphi_{tx} & -S\varphi_{tx} \\ 0 & S\varphi_{tx}/C\varphi_{ty} & C\varphi_{tx}/C\varphi_{ty} \end{bmatrix} \begin{bmatrix} \omega_{tx} \\ \omega_{ty} \\ \omega_{tz} \end{bmatrix} \tag{2}$$

Assumption 1. *The roll angle is small.*

From Assumption 1, $C\varphi_{tx} \approx 1$ and $S\varphi_{tx} \approx 0$; thus, the tilt and pan angles are only coupled by the secant gain $1/C\varphi_{ty}$. The residuals will be treated as mismatched disturbances. It shows that at 0 [deg] of the tilt orientation, the angular rate vector is equal to the vector of Euler angles' rate. However, the greater the tilt orientation, the smaller the yaw rate amplitude compared to the rate of yaw expressed with Euler angles.

Next, we derive the system dynamics from the torque relationships of the inner and outer gimbals by applying Euler's equation of rigid body dynamics. The tilt channel is expressed as:

$$\begin{gathered} \boldsymbol{J_t}\dot{\boldsymbol{\omega}}_{\boldsymbol{t}} + [\boldsymbol{\omega_t} \times \boldsymbol{J_t}\boldsymbol{\omega_t}] = \boldsymbol{T_t} \\ \boldsymbol{J_t} = \begin{bmatrix} J_{tx} & 0 & 0 \\ 0 & J_{ty} & 0 \\ 0 & 0 & J_{tz} \end{bmatrix}, \ \boldsymbol{T_t} = \begin{bmatrix} T_{tx} \\ T_{ty} \\ T_{tz} \end{bmatrix} - \begin{bmatrix} 0 \\ T_{tfc} \\ 0 \end{bmatrix} \end{gathered} \tag{3}$$

where $\boldsymbol{J_t}$ is the inertia matrix of the tilt channel. Assuming that the rotation axes are aligned with the principal axes of inertia, the inertia matrix is, thus, diagonal. $\boldsymbol{T_t}$ is the applied torque consisting of the driving torque from the actuator T_{ty}, the reaction torques T_{tx} and T_{tz} and the friction torque T_{fc}. The dynamics of the tilt channel about the $\boldsymbol{Y}_t$-axis yields the following:

$$J_{ty}\dot{\omega}_{ty} + K_t\omega_{ty} = T_{ty} - (J_{tx} - J_{tz})\omega_{tx}\omega_{tz} + K_t\omega_{py} \tag{4}$$

where K_t is the viscous friction coefficient.

In the same manner, the dynamics of the pan channel are given by:

$$\begin{gathered} \boldsymbol{J_p}\dot{\boldsymbol{\omega}}_{\boldsymbol{p}} + \left[\boldsymbol{\omega_p} \times \boldsymbol{J_p}\boldsymbol{\omega_p} + \boldsymbol{T_{T/P}}\right] = \boldsymbol{T_p} \\ \boldsymbol{J_p} = \begin{bmatrix} J_{px} & 0 & 0 \\ 0 & J_{py} & 0 \\ 0 & 0 & J_{pz} \end{bmatrix}, \ \boldsymbol{T}_p = \begin{bmatrix} T_{px} \\ T_{py} \\ T_{pz} \end{bmatrix} - \begin{bmatrix} 0 \\ 0 \\ T_{pfc} \end{bmatrix}, \ \boldsymbol{T_{T/P}} = {}^{\boldsymbol{P}}\boldsymbol{R_T}\boldsymbol{T_t} = \begin{bmatrix} C\theta & 0 & S\theta \\ 0 & 1 & 0 \\ -S\theta & 0 & C\theta \end{bmatrix}\boldsymbol{T_t} \end{gathered} \tag{5}$$

where $\boldsymbol{\omega_p}$ is the angular rate vectors of the pan channel, and $\boldsymbol{J_p}$ is the inertia matrix of the pan channel. $\boldsymbol{T_p}$ is the applied torque, $\boldsymbol{T_{T/P}}$ is the tilt gimbal torque as observed from the coordinate frame of the pan gimbal, and T_{pfc} is the friction torques of the pan channel. Since the pan channel only controls the motion about the Z_p-axis, the resulting motion equation is:

$$J_{pz}\dot{\omega}_{pz} + (J_{py} - J_{px})\omega_{px}\omega_{py} + T_{T/Z_p} = T_{pz} - K_p\omega_\psi \tag{6}$$

Taking Equation (1) into account, Equation (6) expressed in the coordinate frame fixed to the tilt channel with the variable ω_{tz} instead of ω_{pz} is given as follows:

$$\begin{aligned} &\left(J_{pz} + J_{tx}S^2\theta + J_{tz}C^2\theta\right)\dot{\omega}_{tz} + K_p\omega_{tz} = C\theta T_{pz} + K_p\left(\omega_{px}S\theta + \omega_{bz}\omega_{bz}\right) - J_{pz}\left(-\dot{\omega}_{px}S\theta - \omega_{px}\dot{\theta}C\theta + \omega_{pz}\dot{\theta}S\theta\right) \\ &+\left[J_{tx}\left(\dot{\omega}_{px}C\theta - \omega_{px}\dot{\theta}S\theta - T\theta\left(-\dot{\omega}_{px}S\theta - \omega_{px}\dot{\theta}C\theta\right) - \frac{\dot{\theta}}{C^2\theta}\left(\omega_{tz} - \omega_{px}S\theta\right)\right) + (J_{tz} - J_{ty})\omega_{ty}\omega_{tz}\right]S\theta C\theta \\ &-\left[(J_{ty} - J_{tx})\omega_{tx}\omega_{ty}\right]C^2\theta - C\theta(J_{py} - J_{px})\omega_{px}\omega_{py} \end{aligned} \tag{7}$$

As seen in Equations (1), (2), (4) and (7), the kinematics and dynamics of the 2-axis gimbal system are highly nonlinear and significantly influenced by couplings and external disturbances.

2.2. Actuation Model

A networked real-time control system is used to operate the gimbal system. Two servo actuators—each one integrates a stepping motor, a magnetic encoder, and an inner controller—actuate the two channels of the gimbal independently. The input signal for each actuator is the rate command from the main controller transmitted by an RS-232 communication network. Inside the servo actuators, proportional controllers for speed control are used, so the driving torques are the results of:

$$\begin{aligned} T_{ty} &= P_t(\omega_{\theta d} - \omega_\theta) + d_t \\ T_{pz} &= P_p\Big(\omega_{\psi d} - \omega_\psi\Big) + d_p \end{aligned} \tag{8}$$

where P_t and P_p are the proportional control gains, $\omega_{\theta d}$ and $\omega_{\psi d}$ are the rate commands, d_t and d_p are the unknown disturbances.

Furthermore, in this system, sensors and actuators share a common communication network. Since controller outputs and the data from sensors are simultaneously transmitted, a transmission delay occurs. That is, there exists a time lag from the sensors to the controller and from the controller to the integrated actuators. As a result, the system behaves as an input-delay system where the actual control signal acting on the actuators at a certain time is the delayed version of the one computed. Let the delay time be h, then at the time t, the acting control input was computed at (t–h). Hence, the system model from Equations (1), (2), (4), (7) and (8) can now be rewritten as in Equation (9). (The term indicating the current time t is omitted in the remainder of the article).

$$\begin{aligned} \boldsymbol{A}\dot{\boldsymbol{\varphi}} &= \boldsymbol{\omega} \\ \dot{\boldsymbol{\omega}} &= \boldsymbol{B}\boldsymbol{u}(t-h) - \boldsymbol{K}\boldsymbol{\omega} + \boldsymbol{d} \end{aligned} \tag{9}$$

where $\boldsymbol{\varphi} = \begin{bmatrix} \varphi_{ty} & \varphi_{tz} \end{bmatrix}^T$ is the angular position of the tilt and pan channels expressed in terms of Euler angles. $\boldsymbol{\omega} = \begin{bmatrix} \omega_{ty} & \omega_{tz} \end{bmatrix}^T$ is the angular rate vector. The varying diagonal matrix $\boldsymbol{A} = diag\{A_1, A_2\}$ expresses the relationship between the angular rates and the rates of the Euler angles. $\boldsymbol{u}(t-h)$ is the rate command vector, $\boldsymbol{K} = diag\{K_1, K_2\}$ and $\boldsymbol{B} = diag\{B_1, B_2\}$ are system parameters, and $\boldsymbol{d} = [d_1\ d_2]^T$ is the vector of unpredicted disturbances. These parameters are expressed as:

$$A_1 = 1,\ A_2 = C\varphi_{ty}$$

$$K_1 = \frac{K_t + P_t}{J_{ty}},\ K_2 = \frac{K_p}{J_{pz} + J_{tz}C^2\theta + J_{tx}S^2\theta},$$

$$B_1 = \frac{P_t}{J_{ty}},\ B_2 = \frac{P_pC\theta}{J_{pz} + J_{tz}C^2\theta + J_{tx}S^2\theta},$$

$$d_1 = \frac{1}{J_{ty}}\left(d_t - (J_{tx} - J_{tz})\omega_{tx}\omega_{tz} + (K_t + P_t)\omega_{py}\right)$$

$$\begin{aligned} d_2 = \frac{1}{J_{pz} + J_{tz}C^2\theta + J_{tx}S^2\theta}\Big\{ & d_p + \left(K_p + C\theta P_p\right)\left(\omega_{px}S\theta + \omega_{bz}C\theta\right) - J_{pz}\Big(-\dot{\omega}_{px}S\theta - \omega_{px}\dot{\theta}C\theta + \omega_{pz}\dot{\theta}S\theta\Big) - C\theta P_p\omega_{tz} - C\theta(J_{py} - J_{px})\omega_{px}\omega_{py} \\ & + \Big[J_{tx}\left(\dot{\omega}_{px}C\theta - \omega_{px}\dot{\theta}S\theta - T\theta\Big(-\dot{\omega}_{px}S\theta - \omega_{px}\dot{\theta}C\theta\Big) - \frac{\dot{\theta}}{C^2\theta}\left(\omega_{tz} - \omega_{px}S\theta\right)\right) + (J_{tz} - J_{ty})\omega_{ty}\omega_{tz}\Big]S\theta C\theta - \Big[(J_{ty} - J_{tx})\omega_{tx}\omega_{ty}\Big]C^2\theta\Big\} \end{aligned}$$

3. Control System Design

The common objective of a gimbal control system is to stabilize the LOS and steer it in the desired direction. In this study, the tracking performance is required to be highly accurate, that is, the gimbal system has to follow the reference trajectory in real time with a minimum steady-state error. However, with nonlinearities and disturbances affecting the system performance and the input delay time, the controllable range of the system is limited. Therefore, a backstepping control system is designed in this section to preserve system stability. Furthermore, an extra step is proposed to help cope with the control error

due to delay time. Besides, an STSMC is discussed, and its performance is compared to that of the proposed controller.

3.1. Nonlinear Backstepping Controller Design

3.1.1. Tracking Controller Design

Let the tracking error be defined as:

$$\boldsymbol{e}_{\varphi} = \boldsymbol{\varphi}_d - \boldsymbol{\varphi} \tag{10}$$

where $\boldsymbol{\varphi}_d$ is the desired angular position expressed in terms of Euler angles. Additionally, let the first Lyapunov candidate and its time derivative be as the following:

$$\begin{array}{c} V_1 = \frac{1}{2}\boldsymbol{e}_{\varphi}^T\boldsymbol{e}_{\varphi} > 0 \\ \dot{V}_1 = \boldsymbol{e}_{\varphi}^T\dot{\boldsymbol{e}}_{\varphi} = \boldsymbol{e}_{\varphi}^T(\dot{\boldsymbol{\varphi}}_d - \dot{\boldsymbol{\varphi}}) \end{array} \tag{11}$$

A pseudo control for the Euler angles rate can be chosen as:

$$\boldsymbol{\beta} = \dot{\boldsymbol{\varphi}}_{\boldsymbol{d}} + \boldsymbol{\Lambda}\boldsymbol{e}_{\boldsymbol{\varphi}} \tag{12}$$

where $\boldsymbol{\Lambda}$ is a positive definite diagonal matrix that guarantees the condition of negativity of $\dot{V}_1$. Next, a stabilization error is given as:

$$\boldsymbol{e}_{\boldsymbol{\omega}} = \boldsymbol{A}\boldsymbol{\beta} - \boldsymbol{\omega} \tag{13}$$

which can be understood as the difference between the angular rates computed from the pseudo-Euler angles rates and the actual angular rates of the system. From Equations (12) and (13), the time derivative of the tracking error can be rewritten as:

$$\dot{\boldsymbol{e}}_{\boldsymbol{\varphi}} = \boldsymbol{A}^{-1}\boldsymbol{e}_{\boldsymbol{\omega}} - \boldsymbol{\Lambda}\boldsymbol{e}_{\boldsymbol{\varphi}} \tag{14}$$

Additionally, the time derivative of $\boldsymbol{e}_{\boldsymbol{\omega}}$ is given as:

$$\dot{\boldsymbol{e}}_{\boldsymbol{\omega}} = \frac{\partial}{\partial t}(\boldsymbol{A}\boldsymbol{\beta}) - \boldsymbol{B}\boldsymbol{u}(t-h) - \boldsymbol{d} + \boldsymbol{K}\boldsymbol{\omega} \tag{15}$$

where

$$\begin{array}{c} \frac{\partial}{\partial t}(\boldsymbol{A}\boldsymbol{\beta}) = \boldsymbol{A}\ddot{\boldsymbol{\varphi}}_{\boldsymbol{d}} + \boldsymbol{A}_{\boldsymbol{d}}\dot{\boldsymbol{\varphi}}_{\boldsymbol{d}} + \left(\boldsymbol{A}_{\boldsymbol{d}}\boldsymbol{\Lambda} - \boldsymbol{A}\boldsymbol{\Lambda}^2\right)\boldsymbol{e}_{\boldsymbol{\varphi}} + \boldsymbol{A}\boldsymbol{\Lambda}\boldsymbol{A}^{-1}\boldsymbol{e}_{\omega} \\ \boldsymbol{A}_{\boldsymbol{d}} = \dot{\boldsymbol{A}} = \begin{bmatrix} 0 & 0 \\ 0 & -\dot{\varphi}_{ty}S\varphi_{ty} \end{bmatrix} \end{array} \tag{16}$$

Theorem 1. *The gimbal system controlled by the nonlinear backstepping control (BC) given by Equation (17), namely α, with the proper choice of gains, is input to state (ISS) stable.*

$$\boldsymbol{\alpha} = \frac{\partial}{\partial t}(\boldsymbol{A}\boldsymbol{\beta}) + \boldsymbol{K}\boldsymbol{\omega} + \boldsymbol{A}^{-1}\boldsymbol{e}_{\boldsymbol{\varphi}} + \boldsymbol{\Gamma}\boldsymbol{e}_{\omega} + [sgn(e_{\omega i})]\boldsymbol{\Pi} \tag{17}$$

where $\boldsymbol{\Gamma}$ is a positive definite diagonal matrix, $\boldsymbol{\Pi}$ is a gain vector with positive elements, and $[sgn(e_{\omega i})] = diag\{e_{\omega i}/(|e_{\omega i}| + \delta)\}$ is a diagonal matrix (δ is a positive constant).

Proof of Theorem 1. The control law preserves the system stability in the sense of Lyapunov stability theory by considering the following Lyapunov function candidate:

$$V_2 = V_1 + \frac{1}{2}\boldsymbol{e}_{\boldsymbol{\omega}}^T\boldsymbol{e}_{\boldsymbol{\omega}} > 0 \tag{18}$$

Taking the time derivative of Equation (18) yields:

$$\dot{V}_2 = \dot{V}_1 + \boldsymbol{e}_{\boldsymbol{\omega}}^T \dot{\boldsymbol{e}}_{\boldsymbol{\omega}} = \boldsymbol{e}_{\boldsymbol{\varphi}}^T \left(\boldsymbol{A}^{-1} \boldsymbol{e}_{\boldsymbol{\omega}} - \boldsymbol{\Lambda} \boldsymbol{e}_{\boldsymbol{\varphi}} \right) + \boldsymbol{e}_{\boldsymbol{\omega}}^T \left[\frac{\partial}{\partial t} (\boldsymbol{A}\boldsymbol{\beta}) - \boldsymbol{B}\boldsymbol{u}(t-h) - \boldsymbol{d} + \boldsymbol{K}\boldsymbol{\omega} \right] \tag{19}$$

Additionally, the following expression is considered:

$$\begin{aligned} \boldsymbol{B}\boldsymbol{u}(t-h) &= \boldsymbol{B}\boldsymbol{u} - [\boldsymbol{B}\boldsymbol{u} - \boldsymbol{B}\boldsymbol{u}(t-h)] \\ &= \boldsymbol{B}\boldsymbol{u} - \boldsymbol{\varepsilon} \end{aligned} \tag{20}$$

where the term $\boldsymbol{\varepsilon} = \boldsymbol{B}\boldsymbol{u} - \boldsymbol{B}\boldsymbol{u}(t-h)$ is a well-known expression in the concept of network disturbances, and it is bounded [20]. The delayed input can be then presented as a delay-free one with an additional unknown disturbance. Now, substituting the control law α into $\boldsymbol{B}\boldsymbol{u}$ results in the following:

$$\begin{aligned} \dot{V}_2 &= -\boldsymbol{e}_{\boldsymbol{\varphi}}^T \boldsymbol{\Lambda} \boldsymbol{e}_{\boldsymbol{\varphi}} - \boldsymbol{e}_{\boldsymbol{\omega}}^T \boldsymbol{\Gamma} \boldsymbol{e}_{\boldsymbol{\omega}} + \boldsymbol{e}_{\boldsymbol{\omega}}^T (-[sgn(e_{\omega i})] \boldsymbol{\Pi} + \boldsymbol{\varepsilon} - \boldsymbol{d}) \\ &\leq -\boldsymbol{e}_{\boldsymbol{\varphi}}^T \boldsymbol{\Lambda} \boldsymbol{e}_{\boldsymbol{\varphi}} - \boldsymbol{e}_{\boldsymbol{\omega}}^T \boldsymbol{\Gamma} \boldsymbol{e}_{\boldsymbol{\omega}} + \boldsymbol{e}_{\boldsymbol{\omega}}^T [sign(e_{\omega i})] (-[sgn(|e_{\omega i}|)] \boldsymbol{\Pi} + \lceil |\varepsilon_i - d_i| \rceil) \end{aligned} \tag{21}$$

where the signum matrix $[sign(e_{\omega i})] = diag\{sign(e_{\omega i})\}$ and the matrix $[sgn(|e_{\omega i}|)]$ is given by $diag\{|e_{\omega i}|/(|e_{\omega i}| + \delta)\}$. $\lceil |\varepsilon_i - d_i| \rceil$ denotes a vector whose ith element is $|\varepsilon_i - d_i|$. In the disturbance-free case, i.e., $(\boldsymbol{\varepsilon} - \boldsymbol{d})$ is the zero vector, it is easily seen that the system is asymptotically stable. In general, the stability of the control system is preserved if the value of the third term in Equation (21) is semi-negative. It is easy to see that the aforementioned stability condition is fulfilled if the following is satisfied.

$$|e_{\omega i}| \geq \frac{E_i \delta}{(\pi_i - E_i)}, \ \pi_i > E_i \tag{22}$$

π_i is the ith element of the vector $\boldsymbol{\Pi}$, while E_i is the upper bound of the ith element of $\lceil |\varepsilon_i - d_i| \rceil$. Thus, the time derivative of the Lyapunov candidate in Equation (21) is negative whenever the stabilization error is greater than $E_i \delta / (\pi_i - E_i)$. That is:

$$\dot{V}_2 \leq -\boldsymbol{e}_{\boldsymbol{\varphi}}^T \boldsymbol{\Lambda} \boldsymbol{e}_{\boldsymbol{\varphi}} - \boldsymbol{e}_{\boldsymbol{\omega}}^T \boldsymbol{\Gamma} \boldsymbol{e}_{\boldsymbol{\omega}} \tag{23}$$

A relatively larger value of π_i results in a smaller bound of the error $e_{\omega i}$. The system is ISS stable, and V_2 is the system ISS-Lyapunov function candidate [25]. □

3.1.2. Time Delay Compensator Design

Due to the input delay, the control law acting on the system at a time t is the one computed at the time $t - h$. Therefore, the difference between the computed and the actual control law should be considered. Let us introduce a new error term $\boldsymbol{e}_u$ such that $\boldsymbol{e}_u = \boldsymbol{\alpha} - \boldsymbol{B}\boldsymbol{u}(t-h)$ is the control input error. It represents the difference between the current computed virtual control law and the actual control input to the system.

Assumption 2. *The networked disturbance $\boldsymbol{\varepsilon}$ is a slow time-varying value, i.e., $\dot{\boldsymbol{\varepsilon}} \approx 0$.*

The assumption comes from the bandwidth limitations of a delay system and the properties of practical applications.

Theorem 2. *The feedback control law given in Equation (24) ensures the system ISS stability and reduces the influence of the delay on the system's performance.*

$$\boldsymbol{B}\boldsymbol{u} = \boldsymbol{\alpha} + \boldsymbol{H} \int_0^t \boldsymbol{e}_{\boldsymbol{\omega}}(\tau) d\tau + \boldsymbol{\Omega} \int_0^t \boldsymbol{e}_u(\tau) d\tau \tag{24}$$

$\boldsymbol{H}$ and $\boldsymbol{\Omega}$ are positive definite diagonal matrices.

Proof of Theorem 2. With the introduction of the input error $\boldsymbol{e_u}$, the time derivative of the stabilization error in Equation (15) and the input error are written as follows:

$$\begin{aligned} \dot{\boldsymbol{e}}_\omega &= \boldsymbol{e_u} - \boldsymbol{A}^{-1}\boldsymbol{e}_\varphi - \boldsymbol{\Gamma}\boldsymbol{e}_\omega - \boldsymbol{d} - [sgn(e_{\omega i})]\boldsymbol{\Pi} \\ \dot{\boldsymbol{e}}_u &= \dot{\boldsymbol{\alpha}} - \tfrac{\partial}{\partial t}(\boldsymbol{B}\boldsymbol{u}(t-h)) = \dot{\boldsymbol{\alpha}} - \tfrac{\partial}{\partial t}(\boldsymbol{B}\boldsymbol{u}) \end{aligned} \tag{25}$$

A Lyapunov function candidate and its time derivative are given by:

$$\begin{aligned} V_3 &= V_2 + \boldsymbol{e}_u^T\boldsymbol{H}^{-1}\boldsymbol{e_u} \\ \dot{V}_3 = \dot{V}_2 + \boldsymbol{e}_u^T\boldsymbol{H}^{-1}\dot{\boldsymbol{e}}_u &= -\boldsymbol{e}_\varphi^T\boldsymbol{\Lambda}\boldsymbol{e}_\varphi - \boldsymbol{e}_\omega^T\boldsymbol{\Gamma}\boldsymbol{e}_\omega + \boldsymbol{e}_\omega^T(-[sgn(e_{\omega i})]\boldsymbol{\Pi} - \boldsymbol{d}) + \boldsymbol{e}_u^T\boldsymbol{H}^{-1}\left\{\dot{\boldsymbol{\alpha}} - \tfrac{\partial}{\partial t}[\boldsymbol{B}\boldsymbol{u}] + \boldsymbol{H}\boldsymbol{e}_\omega\right\} \end{aligned} \tag{26}$$

Substituting the control law from Equation (24) into Equation (26) becomes:

$$\dot{V}_3 = -\boldsymbol{e}_\varphi^T\boldsymbol{\Lambda}\boldsymbol{e}_\varphi - \boldsymbol{e}_\omega^T\boldsymbol{\Gamma}\boldsymbol{e}_\omega - \boldsymbol{e}_u^T\boldsymbol{H}^{-1}\boldsymbol{\Omega}\boldsymbol{e_u} + \boldsymbol{e}_\omega^T(-[sgn(e_{\omega i})]\boldsymbol{\Pi} - \boldsymbol{d}) \tag{27}$$

Then, the stability of the system is preserved if the fourth term in Equation (27) is semi-negative. By a similar calculation as in Equation (22), the compact set that every state error trajectory converges to as t $\rightarrow \infty$ is determined as:

$$|e_{\omega i}| < \frac{D_i\delta}{(\pi_i - D_i)},\ D_i \geq |d_i| \tag{28}$$

Outside this set, $\dot{V}_3 < 0$, the system is stable, and the errors converge. Since $D_i < E_i$, the boundedness given by Equation (28) is smaller than the one presented in Equation (22). Therefore, the influence of the delay time on the system performance is reduced, and the precision is enhanced. □

In summary, from Equations (17) and (24), the final control law is a combination of the nonlinear BC law and the time delay compensator. It is designed as in Equation (29) and depicted in Figure 2.

$$\begin{aligned} \boldsymbol{B}\boldsymbol{u} &= \boldsymbol{A}\ddot{\boldsymbol{\varphi}}_d + \boldsymbol{A_d}\dot{\boldsymbol{\varphi}}_d + \boldsymbol{K}\boldsymbol{\omega} + \boldsymbol{C}\boldsymbol{e}_\varphi + \boldsymbol{D}\boldsymbol{e}_\omega + [sign(e_{\omega i})]\boldsymbol{\Pi} + \boldsymbol{H}\int_0^t \boldsymbol{e}_\omega(\tau)d\tau + \boldsymbol{\Omega}\int_0^t \boldsymbol{e_u}(\tau)d\tau \\ \boldsymbol{C} &= \boldsymbol{A_d}\boldsymbol{\Lambda} - \boldsymbol{A}\boldsymbol{\Lambda}^2 + \boldsymbol{A}^{-1},\ \boldsymbol{D} = \boldsymbol{A}\boldsymbol{\Lambda}\boldsymbol{A}^{-1} + \boldsymbol{\Gamma} \end{aligned} \tag{29}$$

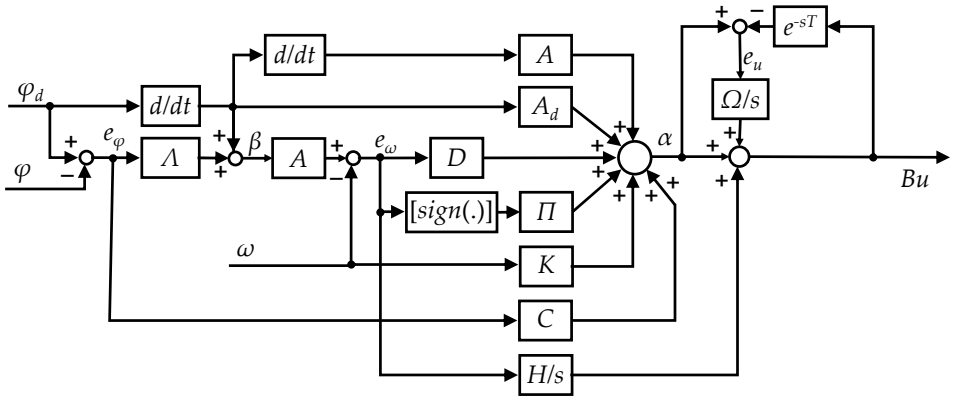

Figure 2. Schematic of the proposed controller.

3.2. Super-Twisting Sliding Mode Control System Design

An STSMC is put to the test in comparison with the proposed controller. Sliding mode strategies are well known for their robustness in facing disturbance. If the nonlinearities—including time-varying parameters, time delay, and external disturbances—are considered as matched and unmatched disturbances, the system description becomes simpler with constant parameters and linear characteristics. In particular, since the roll angles cannot be controlled, their influence on the two other motions can be considered unmatched disturbances. On the other hand, the input delay is somehow a matched disturbance,

along with the dynamic disturbances. Then, the STSMC should be designed such that the control errors remain on a well-behaved sliding manifold despite the presence of model uncertainties and disturbances. The design of the STSMC has been discussed in a previous study [26], where the nominal model of the system is experimentally identified as:

$$\ddot{\boldsymbol{\varphi}} + K\dot{\boldsymbol{\varphi}} = \boldsymbol{Ru} - \boldsymbol{Q\varphi} - \boldsymbol{P} \tag{30}$$

where $\boldsymbol{R} = diag\{B_1, B_2/C\theta\}$. The total effect of external disturbances and neglected terms are experimentally identified as $\boldsymbol{Q\varphi} + \boldsymbol{P}$, where $\boldsymbol{Q}$ is a positive definite diagonal matrix and $\boldsymbol{P}$ is a vector of the remainder. Moreover, the sliding manifold for the two channels is assigned by a vector $\boldsymbol{s}_{STSMC} = \begin{bmatrix} s_1 & s_2 \end{bmatrix}^T = \dot{\boldsymbol{e}}_{\boldsymbol{\varphi}} + \boldsymbol{Me}_{\boldsymbol{\varphi}}$, where $\boldsymbol{M}$ is a positive definite diagonal matrix.

Theorem 3. *The feedback control law is selected based on the following super-twisting algorithm:*

$$\begin{aligned} \boldsymbol{Ru} &= \ddot{\boldsymbol{\varphi}}_{\boldsymbol{d}} + K\dot{\boldsymbol{\varphi}} + \boldsymbol{Q\varphi} + \boldsymbol{Me}_{\boldsymbol{\varphi}} + \boldsymbol{\Theta}\left\lceil |s_i|^{\frac{1}{2}} sign(s_i) \right\rfloor + \boldsymbol{X} \\ \dot{\boldsymbol{X}} &= \boldsymbol{\Xi}\lceil sign(s_i) \rfloor \end{aligned} \tag{31}$$

where $\boldsymbol{\Theta} = diag\{\sigma_1, \sigma_2\}$ *and* $\boldsymbol{\Xi} = diag\{\varsigma_1, \varsigma_2\}$ *are the controller gain matrices.* $\left\lceil |s_i|^{1/2} sign(s_i) \right\rfloor$ *and* $\lceil sign(s_i) \rfloor$ *are vectors whose* i*th elements are* $|s_i|^{\frac{1}{2}} sign(s_i)$ *and* $sign(s_i)$*, respectively. In the sense of the Lyapunov stability theory, with the Lyapunov function candidate for each gimbal channel being proposed as in Equation (32), the control law in Equation (31) preserves the system stability despite the presence of matched and unmatched disturbances with suitable choices of the controller gains* $\boldsymbol{\Theta}$ *and* $\boldsymbol{\Xi}$.

$$V_i = \begin{cases} 2\sqrt{x_i^2 + 3\alpha_i^2\sigma_i^2|s_i|} - x_i sign(s_i) & \text{if } x_i sign(s_i) \leq \alpha_i\sigma_i\sqrt{|s_i|} \\ 3|x_i| & \text{otherwise} \end{cases} \tag{32}$$

Proof of Theorem 3. See [26]. □

4. Simulation and Experimental Studies

In this section, the proposed controller designed in Equation (29) is investigated. By comparing the performance of the STSMC in Equation (31) and the delay-free BC in Equation (17), the efficiency of the proposed control system is evaluated.

The configuration of the target system, the two-axis gimbal, is illustrated in Figure 3.

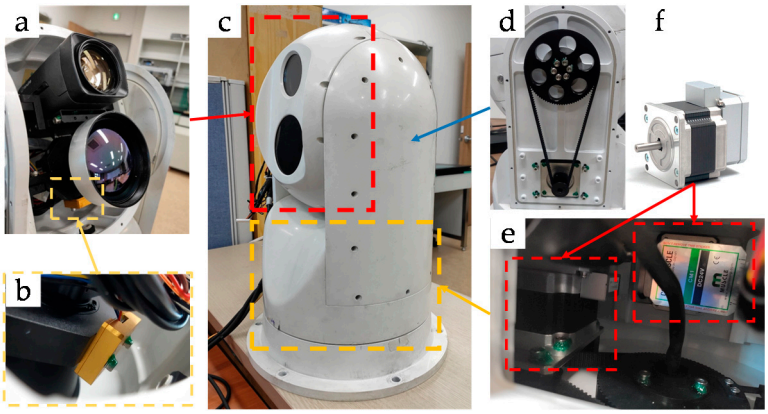

Figure 3. The 2-axis gimbal system apparatus. (**a**) Set of cameras; (**b**) AHRS; (**c**) Overall view of the system; (**d**) Belt and pulley mechanism; (**e**,**f**) Actuators.

First, Figure 3c shows the overall view of the system. The system's payload is a set of cameras, including a vision camera and an infrared thermal imaging camera, as shown in Figure 3a. Their orientations are sensed by an attitude heading reference system (AHRS) attached underneath, Figure 3b. Assembled at the side of the gimbal, a belt and pulley mechanism transmits the rotation from the driving shaft of the tilt actuator to the tilt channel with a reduction ratio (Figure 3e). The actuators are two integrated servo systems COOLMUSCLE CM1-C-23S30—as shown in Figure 3f—each of them is controlled with a rate command sent through the RS-232 communication network. The sampling time of the control system is 0.02 [s], while the average delay time is three times larger, a value identified based on experimental results. Real-time tracking is an important requirement for gimbal systems in ocean surveillance applications. For instance, when the camera in Figure 3a is tracking a faraway moving target, the operator is obliged to zoom in on the target for better visualization. In this case, the field of view of the camera is so small that a small tracking error or a moment of lagging can make the target disappear from the monitor; thus, the tracking fails.

Simulation tests in this study were conducted with the system model introduced in Equation (9) and the proposed controller alongside two others. Furthermore, experimental studies were performed on the target system. The system parameters are shown in Table 1, while the gain matrices of the controllers are presented in Table 2.

Table 1. System parameters.

Parameter	Value
System model (Equation (9))	$\boldsymbol{K} = \begin{bmatrix} 21.9680 & 0 \\ 0 & 30.3969 \end{bmatrix}$, $\boldsymbol{B} = \begin{bmatrix} 22.2485 & 0 \\ 0 & 28.4352C\theta \end{bmatrix}$
System model for STSMC (Equation (30))	$\boldsymbol{R} = \begin{bmatrix} 22.2485 & 0 \\ 0 & 28.4352 \end{bmatrix}$, $\boldsymbol{Q} = \begin{bmatrix} 0.2757 & 0 \\ 0 & 0.0299 \end{bmatrix}$
Delay time	Average 0.06 [s], worst case 0.15 [s]

Table 2. Controller gain matrices.

STSMC (Equation (31))	$\boldsymbol{M} = \begin{bmatrix} 2 & 0 \\ 0 & 1.5 \end{bmatrix}$, $\boldsymbol{\Theta} = \begin{bmatrix} 120 & 0 \\ 0 & 200 \end{bmatrix}$, $\boldsymbol{\Xi} = \begin{bmatrix} 100 & 0 \\ 0 & 100 \end{bmatrix}$
BC (Equation (17))	$\boldsymbol{\Lambda} = \begin{bmatrix} 25 & 0 \\ 0 & 35 \end{bmatrix}$, $\boldsymbol{\Gamma} = \begin{bmatrix} 2.38 & 0 \\ 0 & 2.6 \end{bmatrix}$, $\boldsymbol{\Pi} = \begin{bmatrix} 25 \\ 25 \end{bmatrix}$
Proposed controller (Equation (29))	$\boldsymbol{H} = \begin{bmatrix} 15 & 0 \\ 0 & 5 \end{bmatrix}$, $\boldsymbol{\Omega} = \begin{bmatrix} 10 & 0 \\ 0 & 5 \end{bmatrix}$, $\delta = 5$

4.1. Simulation

In the simulation scenario, the gimbal has to track a mobile target moving along a circular route with different speeds. This task creates the desired trajectories for the tilt and the pan orientations for the inner gimbal given by:

$$\begin{aligned} \varphi_{ty}(t) &= r\sin(2\pi ft) \\ \varphi_{tz}(t) &= r\cos(2\pi ft) \end{aligned} \tag{33}$$

where r is the maximum value of the angle, and f is the desired frequency value in proportion to the target's speed. As abovementioned, the delay limits the bandwidth of the system. Therefore, by performing simulations with a chirp-type reference based on Equation (33), the frequency response and the influence of the time delay are evaluated.

Simulation results are illustrated in Figure 4 in which Figure 4a,b show the frequency responses of the two channels with a delay-free input and a 0.06 [s] delay time, respectively. The responses are drawn from the Fourier transforms of the simulation outputs and the reference signals. This is similar to the concept of the complementary sensitivity function of a linear system, where the magnitude response shows the ratio of the amplitude of the output and the reference, and the phase response indicates the phase lag. The frequency responses of the gimbal system with no delay controlled by the STSMC and the BC are illustrated in Figure 4a. The BC controls the tilt and pan channels accurately in real time with slow-varying reference frequencies up to 1 and 0.8 [Hz], respectively. The values of 0 [dB] in magnitude and 0 [deg] phase shift prove these statements.

On the other hand, using the STSMC, small errors of the amplitude and the phase are seen in the tilt channel response. However, great overshoot and incorrect phase shifts are present in the pan channel response. A possible explanation is the neglect of trigonometric nonlinearities in system dynamics while designing the pan channel controller.

Simulation results of the system with input delay are shown in Figure 4b, and the influence of the time delay is easily noticed. The STSMC, BC, and the proposed controller ensure the results of 0 [dB] and 0 [deg] when following low-frequency trajectories. Thus, accurate tracking performances are achieved both in terms of magnitude and real-time characteristics. However, when the target moves faster, different control performances are obtained from the control schemes. Both the STSMC and the BC perform much worse than they do with the delay-free system. The frequency responses of the tilt channel in Figure 4b show that the controllers based on the backstepping approach increase the bandwidth of the system up to 21% compared to the system controlled by the STSMC. These bandwidths are smaller than the ones shown in Figure 4a, which shows the significant effects of such a small time lag. In their controllable range, the STSMC performs poorly, resulting in the highest magnitude among the three controllers. Starting from 0.2 [Hz] and increasing the frequency, the faster the target becomes, the bigger the amplitude of the system response. Besides, the phase shift begins to decrease at 0.3 [Hz]. Thus, the tracked trajectory using STSMC is far behind the reference. In contrast, the proposed control system provided the most accurate real-time tracking performance on a larger frequency range. The magnitude was maintained at 0 [dB], but starting from 0.4 [Hz], the magnitude began increasing; however, its peak was not higher than that of the BC. The phase lag was also small when the proposed controller was used, as shown in the phase shift plot.

In the case of the pan channel with the input delay, the control bandwidth did not improve much compared to the STSMC. However, both the magnitude and the phase responses improved in the controllable range. Two examples, in particular, illustrate the aforementioned analyses, the frequencies 0.05 and 0.3 Hz, as shown in Figure 4c. These results validate the proposed controller as the one that preserves accurate tracking performance of the system on the largest frequency range.

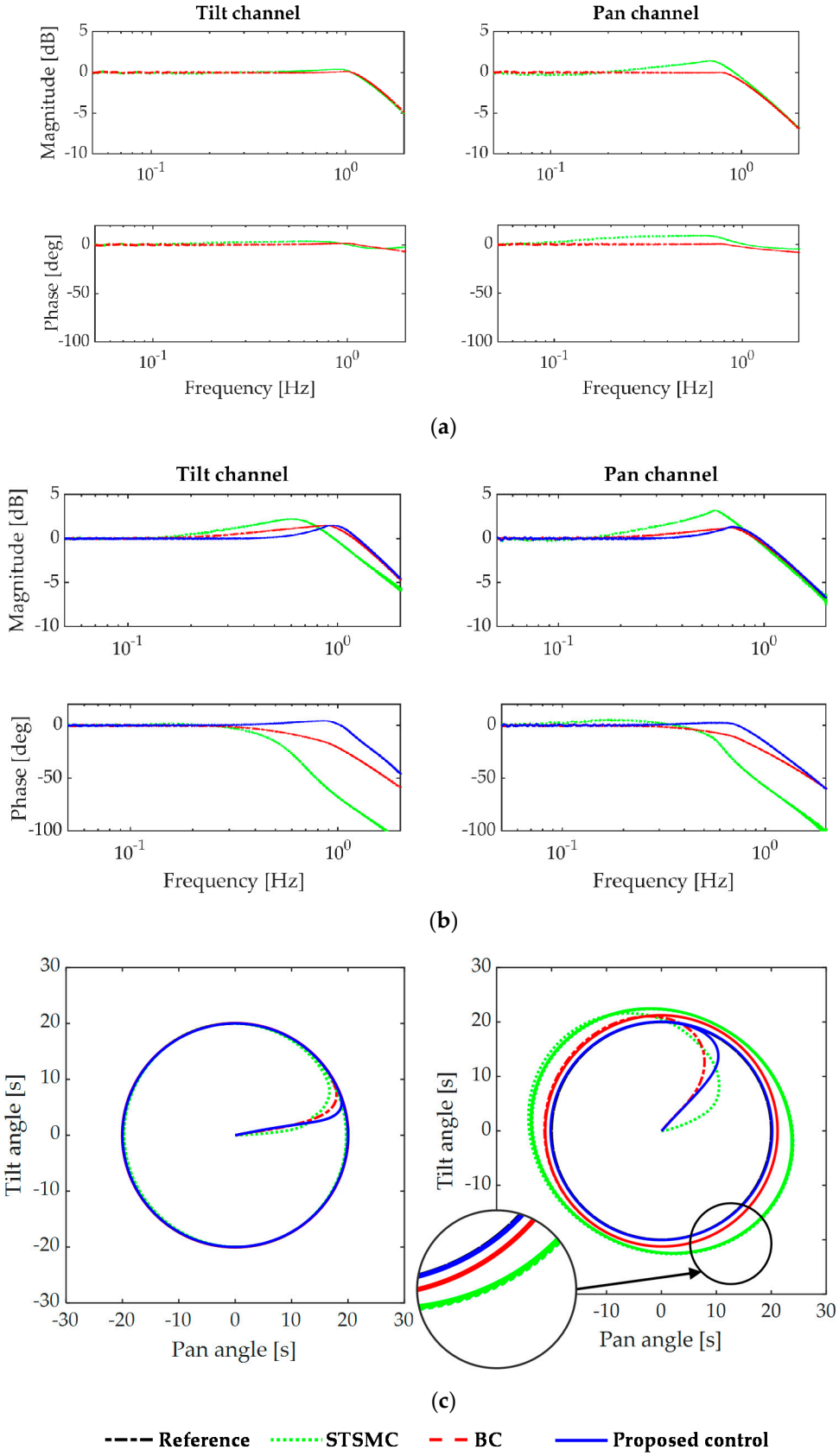

Figure 4. Simulation results. (**a**) Frequency response of the delay-free of the tilt (**left**) and the pan (**right**) channels; (**b**) frequency response of the tilt (**left**) and the pan (**right**) channels with input delay; (**c**) route tracking performance with 0.05 Hz (**left**) and 0.3 Hz (**right**) references.

4.2. Experimental Studies

Experimental studies were performed in two scenarios. The first one is similar to the simulation tests; the gimbal is tracking a moving target. In the second experiment, the system follows step-type references, similar to the point-to-point tracking. Both reference signals are rich in information that help evaluate the effectiveness of the control system.

In the first experiment, the reference signals are chosen as in Equation (33) with a 90 [deg] difference in phase and 20 [deg] in radius. The experiments were conducted on a large frequency range to verify the performance of the system controlled by the proposed controller. Two responses at the specific frequencies 0.05 and 0.3 [Hz] are illustrated geometrically in Figure 5a in a similar fashion to the simulation tests. Details of the time responses of these two frequencies are given in the following Figure 5b,c. The difference between the responses of the two controllers was small in the case of 0.05 [Hz], but the differences are significant with a frequency of 0.3 [Hz]. The time responses in Figure 5b,c indicate that the three controllers were able to attenuate the delay after a few seconds and then track the target in real time (the controllers began to operate the system from the 10th second). However, with 0.3 [Hz], the response given by the STSMC showed a greater overshoot and was slightly lagging behind the reference.

These results correspond with the response illustrated in Figure 4b, where the STSMC gives the highest increase in magnitude and phase lag at 0.3 [Hz]. The proposed controller showed the best performance, as seen in the controlled system response in Figure 5a,b, and a minimal tracking error as shown in Figure 5c. In addition, root-mean-square error values in Table 3 give numerical merits assessing the effectiveness of the proposed controller in comparison with the other control systems.

Table 3. Root-mean-square error [deg].

Trajectory	Channel	STSMC	BC	Proposed
0.05 Hz	Tilt	0.2244	0.1319	0.1037
	Pan	2.0602	2.1586	2.1138
0.3 Hz	Tilt	5.5564	2.2544	1.1699
	Pan	5.8616	2.9772	2.4731

The second experiment was conducted with a step-type reference. The response of each channel is shown individually in Figure 6a,b. The closeup figure at the top right of Figure 6a shows clearly the delayed response. On the other hand, all the controllers were able to control the system to orientate towards the desired positions with no overshoot and small steady-state errors. The closeup figures, in particular, show that the proposed controller provides a better transient response so that the desired positions are reached in a short period of time.

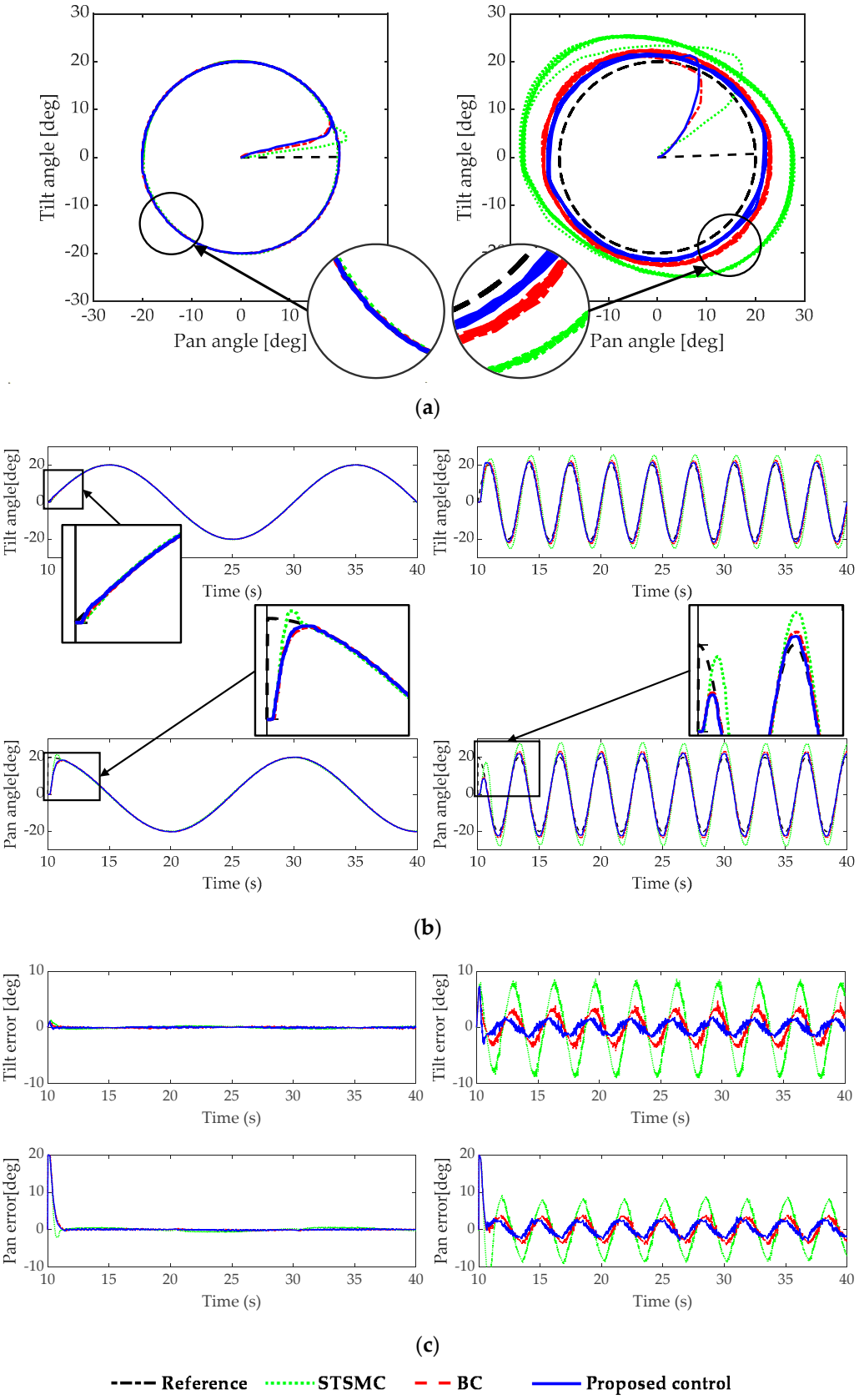

Figure 5. Experimental results with chirp-type references. (**a**) Route tracking performance with 0.05 Hz (**left**) and 0.3 Hz (**right**) references; (**b**) time responses of the tilt (**top**) and the pan (**bottom**) channel with 0.05 Hz (**left**) and 0.3 Hz (**right**) trajectories; (**c**) tracking errors of the tilt (**top**) and the pan (**bottom**) channel with 0.05 Hz (**left**) and 0.3 Hz (**right**) trajectories.

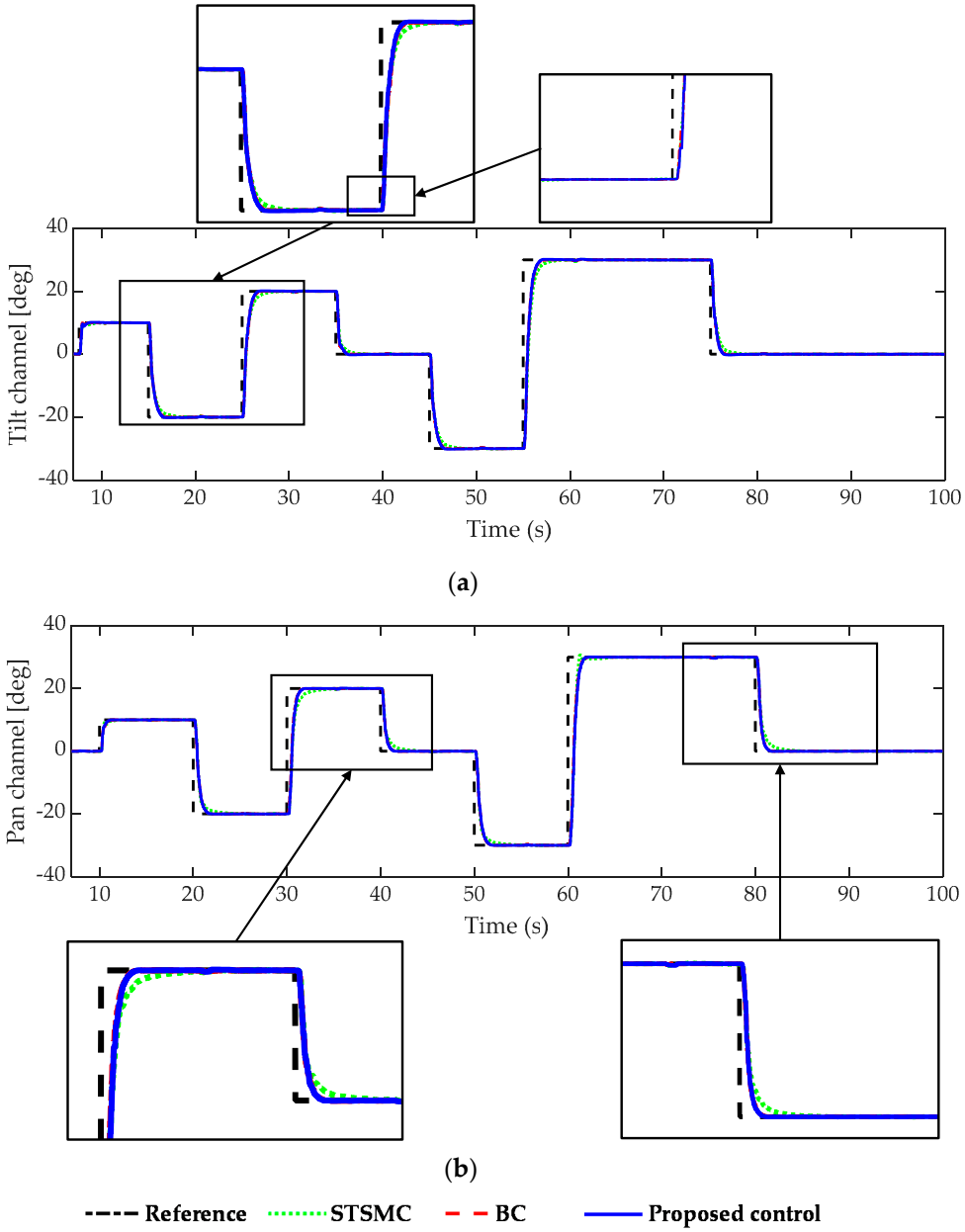

Figure 6. Step response of the gimbal system. (**a**) Time response of the tilt channel; (**b**) time response of the pan channel.

5. Conclusions

A novel nonlinear controller was proposed for a two-axis gimbal system to achieve high precision tracking performance despite the system's nonlinear characteristics and constraints. The paper focused on integrating these factors, mainly delay time, Euler angle-based measurement, and nonlinear dynamics, in the mathematical representation of the system. Then, the designed controller not only preserved the system stability but also achieved high precision tracking performance. Simulations and experiments were conducted providing the system performances in both time and frequency domains. The comparative studies between the proposed controller and the other control systems—including an STSMC and a delay-free BC—proved the superiority of the proposed BC system. The system bandwidth was expanded, and the accuracy and real-time tracking were obtained on a larger range of frequencies. In future works, combining the control system with a mechanism attenuating high-frequency disturbances is going to be studied to enhance the system's accuracy and performance.

Author Contributions: Conceptualization, Y.-B.K.; methodology, T.H.; software, T.H.; validation, H.-C.P., Y.-B.K., and T.H.; formal analysis, Y.-B.K., and T.H.; writing—original draft preparation, T.H.; writing—review and editing, H.-C.P., Y.-B.K., S.C., and T.H. All authors have read and agreed to the published version of the manuscript.

Funding: This research received no external funding.

Institutional Review Board Statement: Not applicable.

Informed Consent Statement: Not applicable.

Data Availability Statement: Data sharing not applicable.

Conflicts of Interest: The authors declare no conflict of interest.

References

1. Hilkert, J. Inertially stabilized platform technology Concepts and principles. *IEEE Control Syst.* **2008**, *28*, 26–46. [CrossRef]
2. Masten, M.K. Inertially stabilized platforms for optical imaging systems. *IEEE Control Syst.* **2008**, *28*, 47–64. [CrossRef]
3. Kennedy, P.J.; Kennedy, R.L. Direct versus indirect line of sight (LOS) stabilization. *IEEE Trans. Control Syst. Technol.* **2003**, *11*, 3–15. [CrossRef]
4. Abdo, M.; Vali, A.R.; Toloei, A.; Arvan, A.T.A.M.R. Research on the Cross-Coupling of a Two Axes Gimbal System with Dynamic Unbalance. *Int. J. Adv. Robot. Syst.* **2013**, *10*, 357. [CrossRef]
5. Mao, J.; Yang, J.; Liu, X.; Li, S.; Li, Q. Modeling and Robust Continuous TSM Control for an Inertially Stabilized Platform with Couplings. *IEEE Trans. Control Syst. Technol.* **2019**, *28*, 2548–2555. [CrossRef]
6. Li, H.; Yu, J. Anti-Disturbance Control Based on Cascade ESO and Sliding Mode Control for Gimbal System of Double Gimbal CMG. *IEEE Access* **2019**, *8*, 5644–5654. [CrossRef]
7. Ding, Z.; Zhao, F.; Lang, Y.; Jiang, Z.; Zhu, J. Anti-Disturbance Neural-Sliding Mode Control for Inertially Stabilized Platform with Actuator Saturation. *IEEE Access* **2019**, *7*, 92220–92231. [CrossRef]
8. Lee, D.-H.; Tran, D.-Q.; Kim, Y.-B.; Chakir, S. A Robust Double Active Control System Design for Disturbance Suppression of a Two-Axis Gimbal System. *Electronics* **2020**, *9*, 1638. [CrossRef]
9. Kurkcu, B.; Kasnakoglu, C.; Efe, M.O. Disturbance/Uncertainty Estimator Based Integral Sliding-Mode Control. *IEEE Trans. Autom. Control* **2018**, *63*, 3940–3947. [CrossRef]
10. Reis, M.F.; Monteiro, J.C.; Costa, R.R.; Leite, A.C. Super-twisting control with quaternion feedback for a 3-DoF inertial stabilization platform. In Proceedings of the 2018 IEEE Conference on Decision and Control (CDC), Miami Beach, FL, USA, 17–19 December 2018; pp. 2193–2198.
11. Sushchenko, O.; Tunik, A. Robust optimization of the inertially stabilized platforms. In Proceedings of the 2012 2nd International Conference "Methods and Systems of Navigation and Motion Control" (MSNMC), Kiev, Ukraine, 9–12 October 2012; pp. 101–105.
12. Baillieul, J.; Antsaklis, P.J. Control and communication challenges in networked real-time systems. *Proc. IEEE* **2007**, *95*, 9–28. [CrossRef]
13. Richard, J.-P. Time-delay systems: An overview of some recent advances and open problems. *Automatica* **2003**, *39*, 1667–1694. [CrossRef]
14. Wook Hyun Kwon, P.G.P. *Stabilizing and Optimizing Control for Time Delay Systems*; Springer: Cham, Switzerland, 2019; ISBN 9783319927039.
15. Zhong, Q.C. *Robust Control of Time-Delay Systems*; Springer: London, UK, 2006; ISBN 9781846282645.
16. Choi, J.-Y.; Krstic, M. Compensation of time-varying input delay for discrete-time nonlinear systems. *Int. J. Robust Nonlinear Control* **2016**, *26*, 1755–1776. [CrossRef]
17. Liao, Y.; Liao, F. Design of a Backstepping Tracking Controller for a Class of Linear Systems with Actuator Delay. *Math. Probl. Eng.* **2015**, *2015*, 160542. [CrossRef]
18. Krstic, M. *Delay Compensation for Nonlinear, Adaptive, and PDE Systems*; Birkhäuser Boston: Cambridge, MA, USA, 2009; ISBN 9780817648763.
19. Zhu, Q.; Zhang, T.; Fei, S. Adaptive tracking control for input delayed MIMO nonlinear systems. *Neurocomputing* **2010**, *74*, 472–480. [CrossRef]
20. Li, Y.-D.; Chen, B. Adaptive neural tracking control for a class of nonlinear systems with input delay and saturation. *Syst. Sci. Control Eng.* **2020**, 1–8. [CrossRef]
21. Chakraborty, I.; Mehta, S.S.; Doucette, E.; Dixon, W.E. Control of an input delayed uncertain nonlinear system with adaptive delay estimation. In Proceedings of the 2017 American Control Conference (ACC), Seattle, WA, USA, 24–26 May 2017; pp. 1779–1784.
22. Chen, J.; Meng, S.; Sun, J. Stability Analysis of Networked Control Systems with Aperiodic Sampling and Time-Varying Delay. *IEEE Trans. Cybern.* **2017**, *47*, 2312–2320. [CrossRef] [PubMed]
23. Qiu, L.; Yang, X.; Ahsan, U.; Pan, J.; Zhang, B.; Yang, R. Model predictive position tracking control for motion system with random communication delay. *IET Control. Theory Appl.* **2020**, *14*, 3515–3525. [CrossRef]

24. Nguyen, C.M.; Tan, C.P.; Trinh, H. State and delay reconstruction for nonlinear systems with input delays. *Appl. Math. Comput.* **2021**, *390*, 125609. [CrossRef]
25. Sontag, E.D. Input to state stability: Basic concepts and results. In *Nonlinear and Optimal Control Theory. Lecture Notes in Mathematics*; Nistri, P., Stefani, G., Eds.; Springer: Berlin/Heidelberg, Germany, 2008; Volume 1932, pp. 163–220. [CrossRef]
26. Huynh, T.; Kim, Y.-B. A Study on Gimbal Motion Control System Design based on Super-Twisting Control Method. *J. Korean Soc. Precis. Eng.* **2021**, *38*, 115–122. [CrossRef]